Nanoscale Horizons

ROYAL SOCIETY OF CHEMISTRY

COMMUNICATION

View Article Online
View Journal

Cite this: DOI: 10.1039/d5nh00563a

Received 6th August 2025,
Accepted 9th October 2025

DOI: 10.1039/d5nh00563a

rsc.li/nanoscale-horizons

Continuous phase hydrophobicity exerts substantial influence on the surface functional group prevalence in protein nanocapsules synthesized in inverse miniemulsion

Carina Jung,[a] Vanja Munk,[a] Xueqing Zhang,[ab] Volker Mailänder†*[ab] and Katharina Landfester †*[a]

Precise control over surface properties is crucial for the design of nanocarriers in biomedical applications. These properties influence biological interactions. Functional co-monomers can be used to tailor the surface chemistry of nanocarriers synthesized in radical heterophase polymerization in aqueous phase. However, achieving similar control over nanocarriers derived from natural materials in inverse miniemulsion, such as protein nanocapsules, remains challenging. Here, we demonstrate how the surface functional group density of protein nanocapsules can be tuned systematically by varying the hydrophobicity of the continuous phase during the synthesis *via* the click reaction between hydrophilic azide-modified proteins and a hydrophobic dialkyne crosslinker. By adjusting the solvent mixture of toluene and cyclohexane, the interfacial properties of the droplets are modified, influencing the partial denaturation of the protein and orientation of the amine-terminated lysine residues. This, in turn, affects the accessibility of the azide groups for the crosslinking. Changes in solvent composition furthermore influence the solubility and reactivity of the crosslinker, thereby modulating the degree of azide functionalization. This allows for precise control over the number of unreacted azide groups available for subsequent biorthogonal click reactions. We demonstrate that the multifunctional surface, with amine, azide and alkyne groups, enables the simultaneous attachment of different molecules to the nanocapsule. Finally, we show that while changes in continuous phase hydrophobicity lead only to minor changes in protein corona composition, they significantly affect macrophage uptake, likely due to differences in surface amine density. Our combined findings provide a novel approach for tailoring the surface functionality of nanocapsules, facilitating more precise and versatile biofunctionalization strategies, particularly for targeted drug delivery.

New concepts

We report a novel concept of adjusting the surface functional group density on protein nanocapsules synthesized in inverse miniemulsion from azide-modified albumin and an alkyne crosslinker. Without the need for post-synthesis functionalization, this method is based on the systematic variation of the hydrophobicity of the continuous phase, which, in turn, affects the protein orientation and availability of the functionalities for crosslinking, as well as the reactivity of the crosslinker. We furthermore demonstrate that the achieved control over surface functional group densities allows for control over cellular interactions, as the cell uptake into macrophages increases significantly with the amount of amine groups present in the capsules. Beyond the control over the functional group density, we also prove the presence of different functional groups on the nanocapsule, and their accessibility for multifunctionalization. We believe that our concept will be crucial for the advancement of protein-based nanocarriers for biomedical application, as it offers an opportunity to fine-tune the level of cellular interaction, and thus a control over the stealth behavior in the unfunctionalized protein nanocapsule and, more importantly, a precise control over the attachment of targeting molecules like antibodies.

1 Introduction

With the rising interest in nanocarriers for nanomedical treatments, gaining a deep understanding of the interactions between nanocarriers and cells has become crucial in the design of such nanocarrier systems. Not only could this understanding lead to an improved design process, but it furthermore bears the potential to introduce properties that allow for a precise control over the cellular uptake.

The intricate nature of the nanocarrier–cell interaction is influenced by numerous factors, which offer possible ways to influence nanocarrier uptake. While the nanocarrier size, shape and surface curvature, as well as composition strongly influence the internalization into cells, chemical surface functionality of a nanocarrier remains a crucial factor in the efficiency of the interaction with cells and the corresponding uptake mechanism.[1]

To influence the nanocarrier uptake into cells, precise control over the surface functionalities, such as amine or other

[a] Max Planck Institute for Polymer Research, Ackermannweg 10, 55128 Mainz, Germany. E-mail: landfester@mpip-mainz.mpg.de, mailaend@mpip-mainz.mpg.de
[b] Department of Dermatology, University Medical Center of the Johannes Gutenberg University Mainz, Langenbeckstr. 1, 55131 Mainz, Germany
† These authors contributed equally as senior authors to the manuscript.

functional groups, is therefore necessary. For conventional polymeric particles obtained by radical polymerization in aqueous emulsion polymerization, this is relatively straightforward, as functional co-monomers can be added in during the synthesis, requiring no additional modification steps in some cases.[2] However, this is not the case for many other nanocarriers, where no radical polymerization is used, and which are obtained by other methods like inverse (mini)emulsion from natural compounds like proteins, frequently necessitating a functionalization post-synthesis.[3]

Beyond the role of nanocarrier functionality in the nano-bio interaction, enhanced control over surface chemistry offers further advantages. Most importantly, influencing the surface functional group density is highly relevant for the controlled surface functionalization of nanocarriers. In the context of nanomedical treatments, the introduction of linkers and subsequent functionalization with targeting moieties like antibodies or nanobodies, which very efficiently target specific cell types, is a possible application for the controlled introduction of surface functionality.[4] Ligand density has been found to be a critical factor when optimizing the efficacy of nanocarriers for nanomedical application.[5] Furthermore, introducing multifunctionality, which would allow for the attachment of a combination of targeting units, may be of great interest in the field of immunotherapy.[6]

Protein nanocapsules consisting of albumins, such as human serum albumin or ovalbumin, as efficient drug delivery systems for immunotherapy are synthesized in inverse miniemulsion, where a crosslinking reaction of the protein occurs exclusively at the water droplet-to-oil interface.[7] While human serum albumin is naturally abundant in the human bloodstream and may lead to a higher biocompatibility, ovalbumin is of interest due to its frequent use as a model antigen in tumor studies.[8] The biorthogonality of the click reaction used to link the protein shell allows for the encapsulation of active ingredients, such as tumor antigens and various adjuvants that stimulate an immune response against the corresponding tumor, in their aqueous center. When equipped with the appropriate adjuvants, even unfunctionalized nanocapsules have been shown to induce complete remission in murine models.[9] An additional control of the surface functionality in this system could offer further advantages *via* the implementation of a targeting functionalization.

For systems such as polystyrene beads or silica nanoparticles, functional groups can be controlled *via* the stochiometry of functional co-monomers, for example aminopropyltriethoxysilane (APTES).[10] In the case of protein-based nanocarriers, however, influencing the functional group density is challenging, as functional groups cannot be added in a controlled manner by introducing co-monomers. Rather, functional groups, most importantly amines, already exist within the proteins in great variety. Successful attempts at influencing the zeta potential have been demonstrated for human serum albumin and silk protein fibroin nanoparticles synthesized by desolvation method. Here, the stochiometry of added crosslinkers like glutaraldehyde or carbodiimides was found to allow for a controlled adjustment of the surface charge.[11] Protein nanocapsules, on the other hand, offer another highly interesting strategy that might allow for an even more detailed control over the surface functional group prevalence: The intricacies of the crosslinking reaction at the water droplet-oil interface render it susceptible to the influence of minor alterations in reaction conditions, such as the hydrophobicity of the organic phase. These alterations can potentially affect the protein orientation, the extent of denaturation, and other factors that might determine the location of specific functional groups within the shell of the final capsule post-crosslinking. The exploration of these effects using methods such as nano differential scanning fluorimetry (NanoDSF) to evaluate protein denaturation, and hansen solubility parameter (HSP) calculations as well as nuclear magnetic resonance (NMR) to investigate the solubility of the crosslinker depending on the organic phase hydrophobicity and its resulting reactivity could potentially enhance our comprehension of both the miniemulsion process and the cellular interactions of protein nanocapsules. Furthermore, it could unveil novel methods of modulating surface chemistry without resorting to post-functionalization techniques.

Katharina Landfester

Congratulations to Nanoscale Horizons on its 10th anniversary! I have been actively publishing in this journal since 2016 and have served as Editorial Board Chair since 2020. It has been inspiring to see how Nanoscale Horizons has grown into a leading platform that unites chemists, physicists, biologists, and engineers in exploring nanoscale phenomena. The journal stands for creativity, excellence, and true interdisciplinarity. I look forward to the next decade, in which Nanoscale Horizons will continue to drive innovation and help shape the future of nanoscience at the interfaces between disciplines. Open Access funding provided by the Max Planck Society.

2 Experimental section

2.1 Materials

Human serum albumin (HSA; ≥97%, agarose) ovalbumin (OVA; ≥98%, agarose), fluorescamine (≥98%), Alexa Fluor 405 NHS ester (AF405-NHS, ≥90%, HPLC), dimethylsulfoxide (DMSO; ≥99.7%), disodium tetraborate decahydrate (99.5%), and Dulbecco's phosphate buffered saline (DPBS) were purchased from Sigma Aldrich. 1-*H*-imidazolesulfurylazide hydrochloride (≥95%, HPLC) was purchased from Biosynth. Alexa Fluor 488 dibenzocyclooctyne (AF488-DBCO, ≥90%, HPLC) and Alexa Fluor 488 Azide (AF488-N_3, ≥90%, HPLC) were purchased from Jena Bioscience. Cyanine 5 sulfo azide

(Cy5-sulfo-N_3, ≥90%, HPLC) was purchased from Lumiprobe. Glycine (≥99%) and sodium dodecyl sulfate (SDS; ≥99.3%) were purchased from Carl Roth. Cy5-oligo (oligo sequence: CCACUCCUUUCCAGAAAACU, modification with Cy5 at 5′ end) was custom-ordered from Eurofins Genomics. Cyclohexane (≥99.5%, GC) was purchased from VWR Chemicals. Toluene (≥99.8%) was purchased from Fisher Scientific. Sodium hydroxide solutions were purchased from Honeywell Fluka. Fetal bovine serum (FBS), β-mercaptoethanol, GlutaMax, penicillin/streptomycin, and Trypsin/EDTA (0.25%) were procured from Gibco. Anthracene azide, $p(E_{53}/B_{40})$-*b*-$p(EO)_{77}$ (poly-[(ethylene-*co*-butylene)-*b*-(ethylene oxide)]) and HDDP (hexanediol-1,6-dipropiolate) were synthesized in house.

2.2 Methods

2.2.1 Synthesis

2.2.1.1 Azidation of human serum albumin. Human serum albumin (HSA, 1 g, 15.02 nmol, 1 eq.) was dissolved in potassium carbonate solution (50 mL, 40 mM in water). Imidazole-1-sulfurylazide hydrochloride (305 mg, 1.46 mmol, 97 eq.) was dissolved in 2 mL water and added dropwise to the protein solution. The reaction mixture was stirred for 30 min, before the pH value was adjusted to 8.3 by adding 2 N $NaOH_{aq}$ and the reaction was stirred for another 23 h. Purification was achieved by dialysis in MilliQ water (3 days), and the product was obtained as a white solid after lyophilization.

2.2.1.2 Azidation of ovalbumin. Ovalbumin (OVA, 1 g, 23.47 nmol, 1 eq.) was dissolved in potassium carbonate solution (50 mL, 40 mM in water). Imidazole-1-sulfurylazide hydrochloride (305 mg, 1.46 mmol, 62 eq.) was dissolved in 2 mL water and added dropwise to the protein solution. The reaction mixture was stirred for 30 min, before the pH value was adjusted to 8.3 byaddition of 2 N $NaOH_{aq}$ and the reaction was stirred for another 23 h. Purification was achieved by dialysis in MilliQ water (3 days), and the product was obtained as a white solid after lyophilization.

2.2.1.3 Nanocapsule synthesis under variation of the crosslinker amount. Nanocapsules were synthesized from 60% human serum albumin azide (HSA-N_3) and 40% ovalbumin azide (OVA-N_3) in inverse miniemulsion, with slight adaptations to what was previously described.[7] Briefly, HSA-N_3 (30 mg) and OVA-N_3 (20 mg) were dissolved in 462 μL $NaCl_{aq}$ and 38 μL Cy5-$oligo_{aq}$. $p(E_{53}/B_{40})$-*b*-$p(EO)_{77}$ (35.7 mg, 9.6 μmol) was dissolved in toluene (8.37 g, 9.61 mL) and added to the aqueous phase. The combined phases were sonicated (pulsed, total time 3 min, 20 s on, 10 s off, 70% amplitude). In the meantime, $p(E_{53}/B_{40})$-*b*-$p(EO)_{77}$ (10.7 mg, 2.9 μmol) and HDDP (various equivalents, see Table S1) were dissolved in toluene (5.58 g, 6.41 mL) to form the crosslinking solution. The sonicated dispersion was heated to 40 °C under constant stirring, and the crosslinking solution was added dropwise. The reaction was stirred at 40 °C overnight. Purification in organic solvent was achieved by centrifugation (2×, 2000*g*, 30 min) and redispersion in cyclohexane. After characterization, 500 μL of the nanocapsule dispersion were redispersed in 5 mL 0.1 wt% SDS_{aq} by dropwise addition of the cyclohexane phase to the aqueous solution under constant shaking (500 rpm) and sonication for 5 min. The resulting dispersion was stirred (room temperature, 900 rpm) overnight and purified by dialysis in water (Amicon filters, 50 kDa MWCO).

2.2.1.4 Nanocapsule synthesis under variation of the solvent composition. Nanocapsules were synthesized from 60% human serum albumin azide (HSA-N_3) and 40% ovalbumin azide (OVA-N_3) in inverse miniemulsion, with slight adaptations to what was previously described.[7] Briefly, HSA-N_3 (30 mg) and OVA-N_3 (20 mg) were dissolved in 462 μL $NaCl_{aq}$ and 38 μL Cy5-$oligo_{aq}$. $p(E_{53}/B_{40})$-*b*-$p(EO)_{77}$ (35.7 mg, 9.6 μmol) was dissolved in mixtures of toluene and cyclohexane (total volume of 9.7 mL) and added to the aqueous phase. The combined phases were sonicated (pulsed, total time 3 min, 20 s on, 10 s off, 70% amplitude). In the meantime, $p(E_{53}/B_{40})$-*b*-$p(EO)_{77}$ (10.7 mg, 2.9 μmol) and HDDP (5 eq. compared to the calculated amount of azide groups) were dissolved in cyclohexane/toluene mixtures of identical composition (total volume 6.4 mL) to form the crosslinking solution. The sonicated dispersion was heated to 40 °C under constant stirring, and the crosslinking solution was added dropwise. The reaction was stirred at 40 °C overnight. Purification in organic solvent was achieved by centrifugation (2×, 2000*g*, 30 min) and redispersion in cyclohexane. After characterization, 500 μL of the nanocapsule dispersion were redispersed in 5 mL 0.1 wt% SDS_{aq} by dropwise addition of the cyclohexane phase to the aqueous solution under constant shaking (500 rpm) and sonication for 5 min. The resulting dispersion was stirred (room temperature, 900 rpm) overnight and purified by dialysis in water (Amicon filters, 50 kDa MWCO).

2.2.2 Analytical methods

2.2.2.1 Infrared spectroscopy (IR). IR spectra of the lyophilized protein samples were measured using an infrared (IR) spectrometer (Bruker Tensor II).

2.2.2.2 Nuclear magnetic resonance (NMR) spectroscopy based analysis of the HSA azidation. ^{1}H NMR spectra were measured in mixtures of 10% D_2O in H_2O at 850 MHz on a Bruker Avance III spectrometer. Briefly, 20 mg (0.3 μmol, 17.7 μmol NH_2) human serum albumin (HSA) and 2.2 mg potassium carbonate were dissolved in the solvent mixture (660 μL). 5.52 mg (26.33 μmol, 1.5 eq.) imidazolesulfurylazide hydrochloride and 0.826 mg (8.778 mmol, 0.5 eq.) dimethylsulfon were dissolved in 100 μL solvent mixture and added to the HSA solution directly before the first measurement. ^{1}H NMR spectra were recorded in regular intervals over the course of several days (176 h).

2.2.2.3 Matrix assisted laser desorption ionization time of flight (MALDI-TOF) analysis. Lyophilized samples were dissolved in water. MALDI-TOF was measured using a Bruker rapifleX MALDI-TOF/TOF mass spectrometer system.

2.2.2.4 Concentration via solid content. 100 μL ($V_{dispersion}$) of the nanocapsule dispersion in water were pipetted into a glass

vial and dried at 80 °C for at least 2 h. The weight of the empty vial, full vial after addition of the dispersion and of the weight of the vial after drying were used to calculate the solid content w% and concentration c of the dispersion as follows:

$$m_{\text{dispersion}} = n_{\text{full vial}} - m_{\text{empty vial}}$$

$$m_{\text{solid}} = m_{\text{after drying}} - m_{\text{empty vial}}$$

$$w\% = \frac{m_{\text{solid}}}{m_{\text{dispersion}}} \times 100\%$$

$$c = \frac{m_{\text{solid}}}{V_{\text{dispersion}}}$$

2.2.2.5 Dynamic light scattering (DLS). Particle sizes were measured on a Zetasizer Nano-S90 device (Malvern) at 20 °C. Cyclohexane/toluene samples were diluted 1 : 50 in the corresponding solvent, water samples were diluted 1 : 15 before measurement. All samples were measured in triplicates (results displayed as mean, SD in error bars if not indicated otherwise).

2.2.2.6 Zeta potential. Zeta potentials were determined using a Zetasizer Nano Z device (Malvern) at 25 °C. All samples were diluted 1 : 10 in 1 mM KCl_{aq} before measurement. All samples were measured in triplicates (results displayed as mean, SD in error bars if not indicated otherwise).

2.2.2.7 Encapsulation efficiency. Encapsulation efficiencies were determined during the purification of the nanocapsules in water by comparing the fluorescence intensities of the flowthrough and original dispersion. Fluorescence intensities were measured using a Tecan Infinite M1000 plate reader (ex. 649 nm/em. 670 nm). The encapsulation efficiency EE% was calculated as follows:

$$\text{EE}\% = \left(1 - \frac{I_{\text{flowthrough}}}{I_{\text{original}}}\right) \times 100\%$$

2.2.2.8 Transmission electron microscopy (TEM). Nanocapsule dispersions were diluted 1 : 50 in the corresponding solvent. The dispersions were dripped onto a carbon grid and air-dried, before measuring on a JEOL JEM1400 transmission electron microscope.

2.2.2.9 Scanning electron microscopy (SEM). Nanocapsule dispersions were diluted 1 : 100 in the corresponding solvent. 2 μL of the dilution were transferred to a silica wafer (PLANO-EM#G3390) and air-dried, before measuring on a Zeiss GeminiSEM 560 device.

2.2.2.10 Nano differential scanning fluorimetry (NanoDSF). NanoDSF was measured at a concentration of 5 mg mL^{-1} in water using a Prometheus NT.48 device (NanoTemper Technologies GmbH). The temperature dependent ratio of the fluorescence intensities at 330 nm and 350 nm was determined for evaluation, as well as the corresponding first derivative.

2.2.2.11 Nuclear magnetic resonance (NMR) spectroscopy-based analysis of the solvent dependent HDDP reactivity. Nanocapsules were prepared as described under **2.2.2** using 5 equivalents of HDDP for crosslinking, with the exception of using deuterated solvents (cyclohexane-d^{12} and toluene-d^{8}) to replace regular cyclohexane and toluene. Directly after addition of the crosslinker, 600 μL of the reaction mixture were transferred into an NMR tube. ^{1}H NMR spectra were measured at 40 °C on a Bruker 700 MHz AvanceIII spectrometer every 20 min over the course of 24 h.

2.2.2.12 Liquid chromatography mass spectrometry (LC-MS) and evaluation. LC-MS measurements were performed using a nanoACQUITY UPLC system coupled to a Synapt G2-Si mass spectrometer. Peptide samples were diluted with with 0.1% formic acid. Hi3 *E. coli* (Waters, Germany) was added at a concentration of 50 fmol μL^{-1} for absolute protein quantification.[12] A nanoACQUITY system containing a C18 analytical reversed phase column (1.7 μm, 75 μm × 150 mm) and a C18 nanoACQUITY trap column (5 μm, 180 μm × 20 mm) was used. Mobile phase A consists of 0.1% (v/v) formic acid in water and mobile phase B of 0.1% (v/v) formic acid with acetonitrile. For separation a gradient of 2% to 37% of mobile phase B over 70 min was used. The UPLC system was coupled to a Synapt G2-Si mass spectrometer performing electrospray ionization (ESI) in positive ion mode using a NanoLockSpray source. The samples were injected with a flow rate of 0.3 μL min^{-1} and Glu-Fibrinopeptide (150 fmol μL^{-1}) and Leu-Enkephalin (200 pg μL^{-1}) were used as reference. The mass spectrometer was operated in resolution mode and data-independent acquisition (MS^{E}) experiments were carried out. The data was acquired using MassLynx 4.2. Proteins were analyzed using Progenesis QI 2.0 (thresholds for noise reduction were set at 120, 25, and 750 counts for low energy, high energy, and peptide intensity) and identified based on a reviewed database downloaded from Uniprot. For protein identification, at least two assigned peptides and five assigned fragments are required. The peptide identification needs three assigned fragments.

To identify proteins, a reviewed human database (Uniprot) was downloaded and analysis was carried out with Progenesis QI (2.0). Parameters for protein identification were set as described before.[13] The human database was modified with the sequence information of Hi3 *E. coli* standard for absolute protein quantification. Additionally, the sequence of ovalbumin was included in the database to accommodate the specific composition of the sample. The amount of each protein in fmol was obtained *via* the TOP3/Hi3 approach.[14]

2.2.2.13 Flow cytometry. Flow cytometric experiments were performed on an Attune™ NxT flow cytometer (Thermo Fisher Scientific). The signals were recorded using the RL1 channel for Cy5 (excitation at 637 nm, band pass filter 670/14 nm). Cell debris was excluded in the Attune™ NxT software by selection of a cell population in the FSC/SSC scatter plot. The percentage of dye-positive cells and the corresponding median fluorescent intensity (MFI) were considered for the evaluation.

2.2.3 Functional group detection

2.2.3.1 Amine group detection via fluorescamine assay. Glycine was dissolved in PBS to form a 1 mM stock solution and a series of standards was formed by continuous dilution. Furthermore, a stock solution of fluorescamine in acetone (0.3 mg mL^{-1}) was prepared freshly. For solid samples, 0.5 mg mL^{-1} solutions were prepared; capsule dispersions were used without further dilution. 10 μL of the standards and samples, respectively, were mixed with 290 μL borate buffer (0.1 M, pH 9.5). The fluorescence of the standards and samples was determined as follows: To the solution in borate buffer (total volume of 300 μL), 100 μL of the fluorescamine stock solution were added, and the mixture was vortexed for 30 s. Triplicates of 100 μL each were transferred into a black 96-well plate and measured directly using a Tecan Infinite M1000 platereader (ex. 410 nm/em. 470 nm). The amine concentration of the samples was calculated from the fluorescence intensities using the calibration curve formed by the standards.

2.2.3.2 Azide group detection via AF488-DBCO. Azide groups were quantified by reaction with AF488-DBCO. All capsule dispersions were diluted to the same concentration (0.69 mg mL^{-1}) in water. AF488-DBCO was dissolved in DMSO (5 mg mL^{-1}). 6 μL of this solution (30 μg, 37.8 nmol, 1 eq.) were added to 194 μL (133 μg, 2.3 nmol protein with 37.8 nmol azide groups according to MALDI-TOF, 1 eq.) to reach a total volume of 200 μL. The reaction mixtures were shaken (500 rpm, 20 °C) overnight. To determine the amount of reacted dye, a standard curve was prepared using a concentration series of the AF488 dye. The samples were centrifuged (5000 rpm, 30 min), and 100 μL of the supernatants were removed for measurement. The fluorescence of the concentration series and the supernatants was measured using a Tecan Infinite M1000 platereader (ex. 488 nm/em. 517 nm). Using the calibration curve, the concentration of the supernatants, and the amount of azide groups in the supernatant was determined. The azide amount on the capsules was calculated as the difference between the total amount added and the amount detected in the supernatant.

2.2.3.3 Alkyne group detection via AF488-N_3. Alkyne groups were quantified by reaction with AF488-N_3. All capsule dispersions were diluted to the same concentration (0.69 mg mL^{-1}) in water. AF488-N_3 was dissolved in water (2 mg mL^{-1}). 13.1 μL of this solution (26.2 μg, 37.8 nmol, 1 eq.) were added to 187 μL (133 μg, 2.3 nmol protein with originally 37.8 nmol azide groups according to MALDI-TOF, 1 eq.) to reach a total volume of 200 μL. The reaction mixtures were shaken (500 rpm, 20 °C) for 48 h. To determine the amount of reacted dye, a standard curve was prepared using a concentration series of the AF488 dye. The samples were centrifuged (5000 rpm, 30 min), and 100 μL of the supernatants were removed for measurement. The fluorescence of the concentration series and the supernatants was measured using a Tecan Infinite M1000 platereader (ex. 488 nm/em. 517 nm). Using the calibration curve, the concentration of the supernatants, and the amount of alkyne groups in the supernatant was determined. The alkyne amount on the capsules was calculated as the difference between the total amount added and the amount detected in the supernatant.

2.2.3.4 Calculation of amine/azide/alkyne groups per surface area. The number of groups per surface area was calculated as follows: Using the capsule diameter as determined by DLS, the surface area per nanocapsule (A_{NC}) and the volume of one nanocapsule (V_{NC}) were calculated:

$$A_{NC} = 4\pi\left(\frac{d_{NC}}{2}\right)^2 \quad V_{NC} = \frac{4}{3}\left(\frac{d_{NC}}{2}\right)^3$$

For each synthesis, a total mass (m_{total}) of 50 mg protein (30 mg HSA and 20 mg OVA) were dissolved in a total volume (V_{total}) of 500 μL water. The total number of nanocapsules N_{total} was calculated from the total volume and capsule volume as $N_{total} = \frac{V_{total}}{V_{NC}}$.

The results, as determined in nmol mg^{-1}, were used to calculate the total measured amount as $n_{total} = 50c_{measured}$, and the measured amount per nanocapsule:

$$n_{NC} = \frac{n_{total}}{N_{total}}.$$

From this value and the surface area per capsule, the amine amount per area con be calculated as:

$$\text{groups per area} = \frac{n_{NC}}{A_{NC}}$$

2.2.3.5 Multifunctional nanocapsule. For multifunctionalization, a nanocapsule batch was synthesized as described above (**2.2.2**), but without the Cy5-oligo dye. After redispersion and purification, 1 mg nanocapsules were mixed with 2 μL each of AF488-DBCO, AF405-NHS, and Sulfo-Cy5-N_3 (10 μg each, 5 mg mL^{-1} in DMSO), the volume was adjusted with MilliQ water, and the reaction mixture was incubated at rt, 500 rpm overnight. For purification, the NCs were washed repeatedly with MilliQ water using an Amicon 300 kDa MWCO centrifugal filter at 30 min × 500*g*. Once no Cy5 fluorescence was detected in the flowthrough (*via* platereader), indicating a complete purification, the fluorescence and absorption spectra of the unmodified and modified nanocapsules, as well as the corresponding dyes, were recorded using a platereader.

2.2.4 Hansen Solubility Parameter (HSP) Calculations

2.2.4.1 Calculation of the HSP partial parameters for HDDP. Hansen solubility parameters of HDDP were calculated according to E. Stefanis *et al.*[15] Briefly, the partial HSP corresponding to the contributions of dispersion intermolecular forces (δ_d), dipole intermolecular forces (δ_p), and hydrogen-bonding intermolecular forces (δ_h) were calculated from the contributions of the first order groups of HDDP, namely –CH_2– (N = 6), HC≡C– (N = 2),

and –COO– (N = 2), as follows:

$$\delta_d = \left(\sum_i N_i C_i + W \sum_j M_j D_j + 17.3231\right) \mathrm{MPa}^{\frac{1}{2}}$$

$$= \left(\sum_i N_i C_i + 17.3231\right) \mathrm{MPa}^{\frac{1}{2}} = 18.0335\ \mathrm{MPa}^{\frac{1}{2}}$$

$$\delta_p = \left(\sum_i N_i C_i + W \sum_j M_j D_j + 7.3548\right) \mathrm{MPa}^{\frac{1}{2}}$$

$$= \left(\sum_i N_i C_i + 7.3548\right) \mathrm{MPa}^{1/2} = 9.7964\ \mathrm{MPa}^{\frac{1}{2}}$$

$$\delta_h = \left(\sum_i N_i C_i + W \sum_j M_j D_j + 7.9793\right) \mathrm{MPa}^{\frac{1}{2}}$$

$$= \left(\sum_i N_i C_i + 7.9793\right) \mathrm{MPa}^{\frac{1}{2}} = 9.9329\ \mathrm{MPa}^{\frac{1}{2}}$$

with $W = 0$ due to HDDP having no second order groups.

2.2.4.2 Calculation of the HSP partial parameters for solvent mixtures. The HSP partial parameters of the solvent mixtures were calculated from the partial parameters of the pure solvents:

Toluene: $\delta_d = 18.0$; $\delta_p = 1.4$; $\delta_h = 2.0$

Cyclohexane: $\delta_d = 16.8$; $\delta_p = 0.0$; $\delta_h = 0.2$

For the mixtures, the partial parameters were calculated according to the percentages × of the two solvents, *e.g.* $\delta_{d,mix} = x_{toluene}\ \delta_{d,toluene} + x_{cyclohexane}\ \delta_{d,cyclohexane}$. The resulting partial parameters are listed in Table S2.

2.2.4.3 Calculation of the distance R_a. The distance between two substances, of the crosslinker HDDP and a specific solvent mix was calculated as follows:[16]

$$R_a = \sqrt{4(\delta_{d1} - \delta_{d2})^2 + (\delta_{p1} - \delta_{p2})^2 + (\delta_{h1} - \delta_{h2})^2}$$

The calculated R_a values are available in Table S2.

2.2.5 Protein and cell interaction

2.2.5.1 In vitro protein corona in human plasma. Human citrate plasma was obtained from healthy donors at the Transfusion Center of the University Medical Center Mainz. All experiments containing human blood plasma from these donors were approved by the ethics committee of the Landesärztekammer Rheinland-Pfalz, Mainz, Germany No. 837.439.12 (8540-F) and thus performed in compliance with all relevant laws and guidelines. 500 μg nanocarriers were incubated in human plasma at 37 °C (1 h, 300 rpm), and purified by centrifugation (30 min, 20 000*g*, 4 °C) and washing with PBS (2×; removal of the "soft" corona and unbound proteins). The purified sample pellets containing the "hard" corona were resuspended in 100 μL Ampuwa water. The protein corona was quantified by Pierce 660 Assay and evaluated using LC-MS analysis.

2.2.5.2 In solution digestion. Digestion was performed to previously established protocols.[17] The proteins were precipitated using a ProteoExtract protein precipitation kit (CalBioChem), isolated by centrifugation (10 000*g*, 10 min) and suspended with 50 mM RapiGest SF (Waters) in ammonium bicarbonate buffer. 5 mM dithiothreitol (Sigma Aldrich) were added to reduce the proteins (45 min, 56 °C), followed by an alkylation with 15 mM iodoacetamiede (Sigma Aldrich; 1 h, rt). The proteins were digested using 0.02 eq. trypsin at 37 °C for a duration of 16 h. The reaction was quenched with HCl_{aq}. Purification was achieved *via* centrifugation (13 000*g*, 15 min, 4 °C), and the samples were evaluated using LC-MS.

2.2.5.3 Cell culture of J-774A.1. J-774A.1 cells were cultured in Dulbecco's modified Eagle medium (DMEM), supplemented with 10% heat-inactivated FBS, 1% penicillin/streptavidin, and 1% glutamine. The cells were kept at 37 °C and 5% CO_2 in a humidified incubator, using trypsin/EDTA (0.25%) for passaging and harvesting. Viability and cell count were determined from a 1 : 1 dilution with trypan blue using an automated cell counter (TC10, Bio-Rad). The passage was kept below 20 to ensure stability.

2.2.5.4 In vitro cell uptake. 100 000 cells per well were seeded in a 24-well plate and incubated at 37 °C, 5% CO_2 overnight. 250 μg mL^{-1} and 500 μg mL^{-1} nanocarriers were dispersed in medium ($DMEM^{+FBS}$) and 250 μL of the resulting dispersions were added to each well in triplicates. After incubation (18 h at 37 °C), the cells were washed with 1 mL PBS per well to remove excess nanocarriers. 150 μL PBS with 2 mM EDTA and 100 μL Trypsin with 0.25% EDTA were added to collect the cells. The plate was then kept at room temperature for 5 min, before 250 μL $well^{-1}$ medium was added and the samples were transferred into Eppendorff tubes. The media were removed by centrifugation (400*g*, 5 min), and the cell pellet was resuspended in 1 mL PBS for flow cytometry measurements.

2.2.5.5 Cell viability via CellTiter Glo™ assay. 5000 cells per well in 100 μL each were seeded into a white 96-well plate and incubated (37 °C, 5% CO_2) overnight. All samples were diluted identically to the mastermixes used for cell uptake. The media were removed from the wells, and 100 μL $well^{-1}$ of the mastermixes were added in triplicates. The sample was incubated for 18 h. CellTiter Glo™ reagent was added (100 μL $well^{-1}$) to the wells, and the plate was shaken on an orbital shaker for 2 min at room temperature to induce cell lysis. The plate was then incubated at rt for 10 min to stabilize the signal, shaken again for 10 s, and the luminescence (OD1) was detected using a Tecan Infinite M1000 platereader. The signal received from the untreated cells (negative control) was set to 100% viability as a reference.

3 Results and discussion

A multitude of methods exists for influencing the nano-bio interaction, including the introduction of charge *via* functional groups, which has been proven to have a significant impact.[18]

This suggests that the controlled introduction of functional groups might lead to a certain level of control over the cellular interaction of nanocarriers. In addition to modulating surface charge, functional groups play a pivotal role in the attachment of further functionalizations like PEG, linkers, and targeting moieties such as nanobodies or antibodies to the nanocarrier surface.[19]

For most nanocarriers, the introduction of functional groups requires post-synthesis modification, resulting in more intricate systems and extended processes. A more sophisticated approach would be to regulate the properties of nanocarriers as early as during their synthesis, by systematically varying reaction parameters.

In the case of protein click nanocapsules, functional groups like amines are introduced by the presence of proteins in the reaction mixture. By controlling which of these functional groups are facing the surface of the finished protein capsule, precise control of the capsules' surface properties can be achieved. The solvent composition or polarity, which can influence protein orientation during capsule synthesis, and the amount of crosslinking, which can affect the mobility of proteins in the capsule shell and the accessibility of their functional groups post-synthesis, are possible reaction parameters to achieve this control.

A variation of the surface functional groups and the resulting change in the physicochemical identity of the nanocapsules may also influence the protein corona absorption and, consequently, the biological identity. Both physicochemical properties, and protein corona composition can have a significant impact on cellular interaction, possibly allowing for a control over the cell uptake (Fig. 1).

Therefore, we present a study on the systematic variation of reaction conditions during the inverse miniemulsion process of protein nanocapsules and demonstrate that simple changes in the solvent composition lead to a control over the density of amine groups detected on the capsule surface and eventually significantly affect the cell uptake efficiency. The presented conditions offer a simple way of controlling surface properties without post-synthesis modification and offer valuable insights for future functionalization reactions with targeting moieties.

3.1 Synthesis and characterization

As previously described, all protein nanocapsules (NCs) were prepared in an inverse miniemulsion process.[7,20] To allow for a linking of the capsule shell, human serum albumin (HSA) and ovalbumin (OVA) were first modified with azide functionalities. This was achieved by reacting their lysine units with 1*H*-imidazole-1-sulfonyl azide hydrochloride (Imi-N_3) to form azide moieties on the protein (Fig. 2A). The resulting amount of azide groups per protein was calculated for both human serum albumin azide (HSA-N_3) and ovalbumin azide (OVA-N_3) using matrix-assisted laser-desorption-ionization time of flight (MALDI-TOF) mass spectrometry (MS, Fig. 2B), revealing a reaction efficiency of approximately 50%. This efficiency was further confirmed by observation of the reaction by ^{1}H NMR spectroscopy and analysis of the reactant signals in comparison to an internal dimethyl sulfone (DMS) standard (Fig. S1 and S2). As expected, due to the lower overall amount of lysine units per protein, only minor changes were observed using infrared (IR) spectroscopy (Fig. S3 and S4), with a slightly more pronounced stretching vibration of the azide group for HSA-N_3 resulting from the higher amount of initially available lysine units (59 compared to 20 for OVA) in HSA.[21]

After successful modification of the albumins, protein NCs were prepared in inverse miniemulsion, as illustrated in Fig. 2C. 60% HSA-N_3, 40% OVA-N_3, and Cy5-oligo as a fluorescent dye were dissolved in water to form the disperse phase (blue) and mixed with a surfactant-containing organic phase

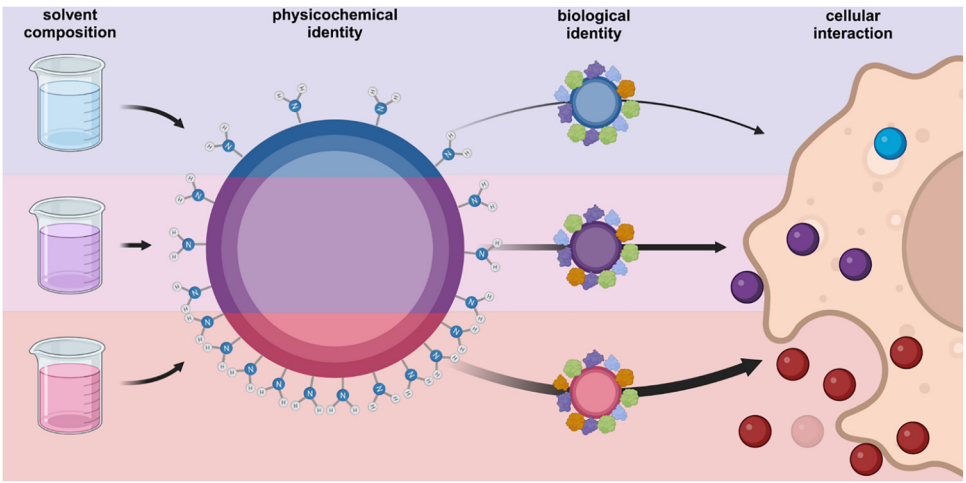

Fig. 1 Concept overview. A variation of the solvent mixture, and consequently hydrophilicity of the organic face in the inverse miniemulsion, bears the potential to influence the orientation of the protein at the water-to-oil interface. Depending on this hydrophilicity-induced orientation, a varying amount of functional groups like amines will be located on the nanocapsule surface after synthesis. Since a variation of the surface functional group density results in a variation of the surface charge itself, the absorbed protein corona and cellular interaction may be influenced significantly. Created in BioRender. Jung, C. (2024) BioRender.com/c94t881.

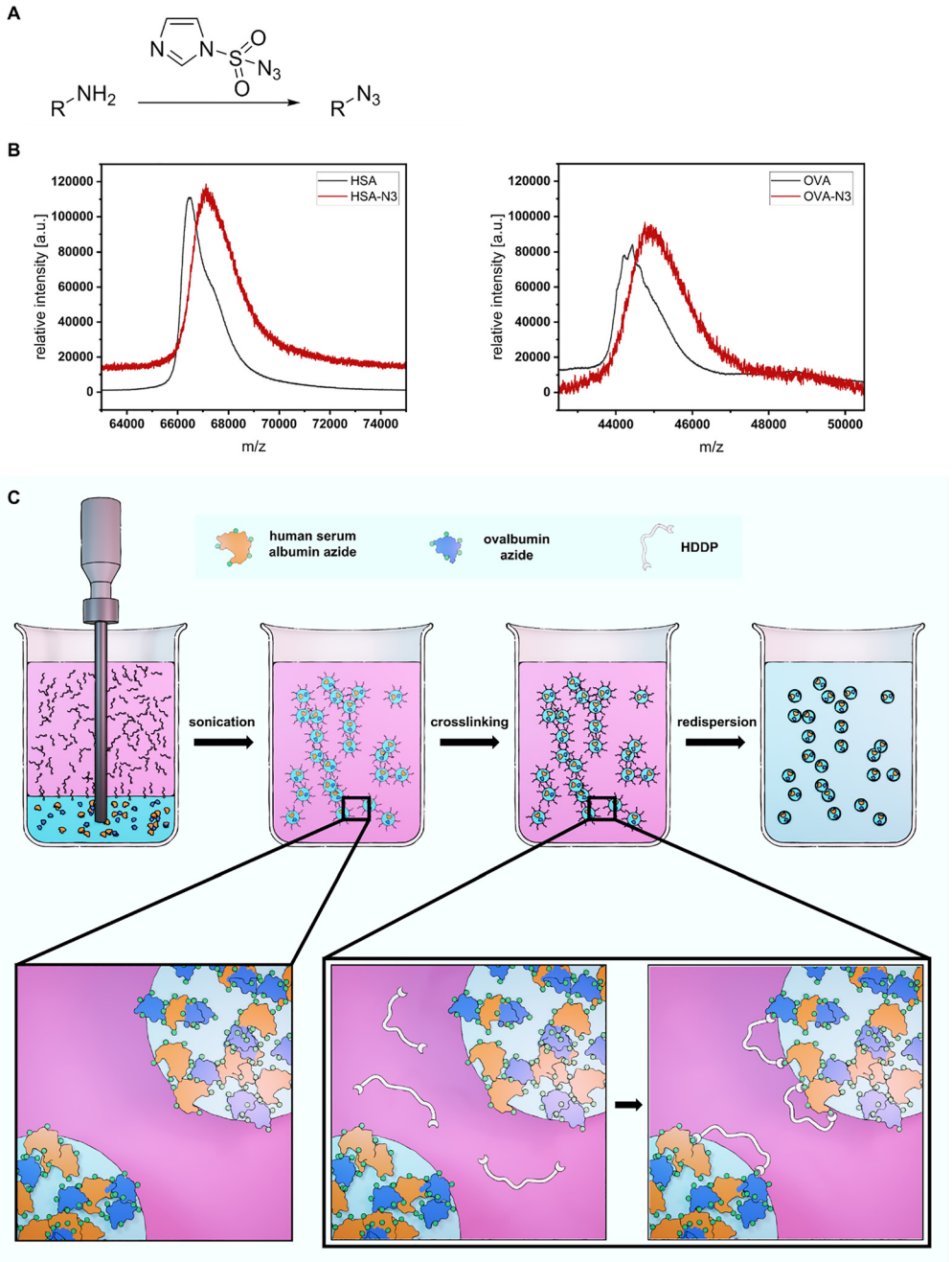

Fig. 2 Preparation of protein nanocapsules from HSA and OVA. (A) Azidation of the albumins. (B) MALDI-TOF evaluation of albumin-azide in comparison to unmodified albumin. (C) Schematic representation of nanocapsule synthesis from 60% HSA-N_3 and 40% OVA-N_3. Miniemulsion process with crosslinking at the interface between the water droplets and the organic solvent.

(continuous phase, colored pink). Following sonication, a crosslinking solution of hexanediol-1,6-dipropiolate (HDDP) was added dropwise, and the reaction was continued overnight. Due to the good solubility of HDDP in the organic phase, and the high solubility of the protein in the aqueous phase, the crosslinking reaction occurs preferably at the interface of the protein droplets, resulting in a nanocapsule with a crosslinked protein shell surrounding a liquid core containing unreacted protein and the fluorescent dye. The biorthogonality of the interfacial click reaction used to link the protein shell furthermore allows for the encapsulation of further active ingredients, as demonstrated in literature.[7] For this reason, the system has been the subject of rising interest for immunotherapeutic applications.

Since biological applications largely require aqueous systems, all capsules were transferred into an aqueous SDS solution. The surfactant was removed, and the capsules were characterized with regards to their physicochemical properties prior to performing further biological studies.

During the synthesis, two parameters majorly influence the capsule formation process: the amount and concentration of

the crosslinker, which can substantially impact the crosslinking density of the protein shell, and the solvent polarity, which affects the solubility and, consequently, the availability of the crosslinker for reaction. An investigation of these two parameters with respect to the properties of the product will facilitate a more profound comprehension of the capsule formation process and enable enhanced fine-tuning of the surface properties of protein nanocapsules in subsequent studies.

3.1.1 Variation of the crosslinker amount. All nanocapsules were prepared from 60% human serum albumin and 40% ovalbumin. To test the impact of variations in the crosslinker amount, the capsules were synthesized in toluene as the organic solvent, and the amount of crosslinker was systematically varied from 25 molar equivalents to 0.1 equivalents alkyne per azide in the batch. The resulting samples were characterized using a variety of analytical methods, including scanning electron microscopy (SEM, Fig. 3A) and transmission electron microscopy (TEM, Fig. 3B), as well as dynamic light scattering (DLS, Fig. S5) and infrared spectroscopy (IR, Fig. S6). These characterizations were performed prior to the redispersion of the samples into the aqueous phase.

A comparison of the electron microscopy images of the samples with the highest and lowest crosslinker amounts reveals minor differences in morphology: In both cases, the collapsed capsule structure is clearly visible, however, lower HDDP concentrations result in a higher polydispersity of the capsule size, with very small structures visible in TEM.

Subsequent to the transfer of the capsules into the aqueous phase, the accessible amine group concentration was determined *via* fluorescamine assay (Fig. 3C, calibration curve in Fig. S7). A clear trend emerges, indicating a maximum accessible amine concentration for the sample prepared with 5 equivalents of crosslinker, with the exception of the sample prepared with very low (0.1) equivalents of crosslinker. In this case, the exceptionally high amine concentration may be attributed to incomplete linking resulting from the utilization of a minimal amount of crosslinker, potentially leading to capsule rupture and the exposure of the amine groups within the shell. Additionally, the small structures visible in TEM may lead to a higher total surface with a consequently higher amount of accessible amine groups. On the other hand, the samples prepared with higher equivalents of HDDP are in danger of experiencing monofunctionalization of proteins, as opposed to crosslinking. This could result in a looser protein network, allowing for rapid penetration by the fluorescamine dye within the capsule. However, a high degree of this monofunctionalization is unlikely even for higher crosslinker concentrations, due to the close proximity of the proteins at the interface.

As amine groups serve as potential anchor points for functionalization reactions, having a sufficient number of accessible amines might be advantageous for capsule modification. Additionally, and more importantly, amine groups may increase surface polarity and influence the interaction with proteins and cells.

Given the relatively high number of amine groups detected and the relatively low amount of crosslinker used for the sample prepared with 5 equivalents of alkyne per azide, all subsequent capsules were prepared with this crosslinker amount.

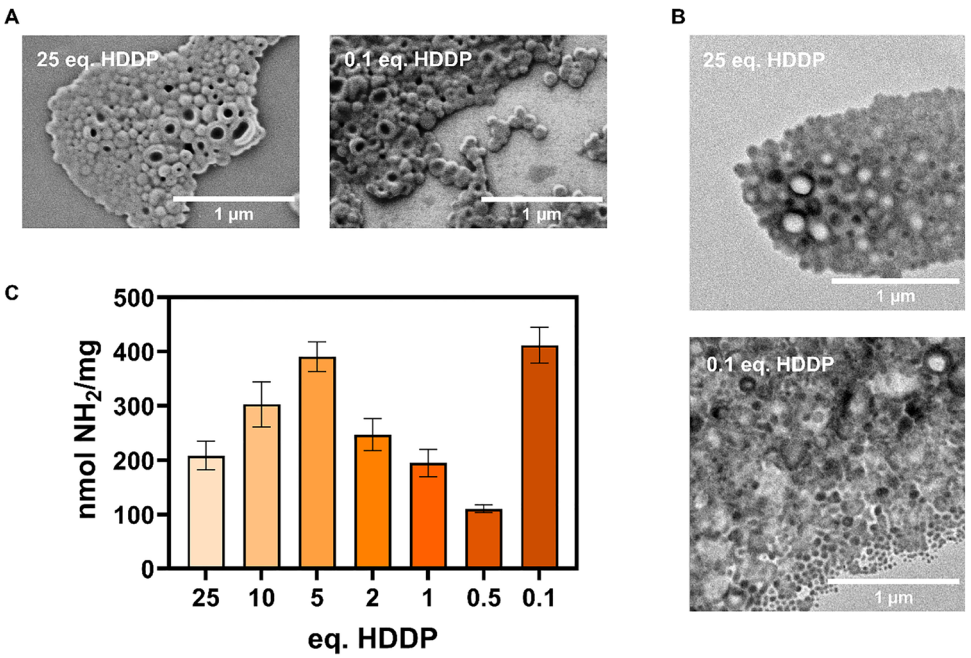

Fig. 3 Characterization of protein nanocapsules synthesized with varying crosslinker amounts. (A) Scanning electron microscopy (SEM) evaluation of the samples with the highest and lowest amount of crosslinker (HDDP). (B) Transmission electron microscopy (TEM) evaluation of the samples with the highest and lowest amount of crosslinker (HDDP). (C) Dependency of the concentration of accessible amine groups on the crosslinker amount, as determined by fluorescamine assay (measured in triplicates, standard deviation (SD) as error bars).

3.1.2 Variation of the continuous phase hydrophobicity. Beyond the crosslinker amount, the solvent polarity may significantly impact capsule properties, as it influences the solubility and, consequently, the availability of the crosslinker. A higher local concentration of the crosslinker at the interface could lead to denser crosslinking of the protein shell. Furthermore, the orientation of proteins at the water-organic solvent interface may be subject to change, influenced by the properties of the surrounding organic solvent, resulting in the exposure of different groups on the capsule surface after linking. Lastly, the solvent polarity may impact the degree of denaturation in the protein.

To investigate the impact of solvent hydrophobicity in the continuous phase, toluene and cyclohexane were mixed in different ratios. Experimentally, the two solvents exhibit vastly different capabilities to dissolve the crosslinker HDDP, with toluene being a much better solvent for this specific molecule (Fig. S8 and S9). The different solubilities could lead to differences in partitioning and reactivity.

After synthesis in the respective solvent mixtures, the resulting nanocapsule samples were investigated using scanning electron microscopy (SEM) and dynamic light scattering (DLS), in order to gain insight into size and morphology trends (Fig. 4, PDI in Table S3). When comparing the SEM images, there are visible trends: Samples produced with 100% toluene exhibited what appeared to be more pronounced edges in the collapsed capsule structures, suggesting either a more rigid protein shell, potentially resulting from enhanced crosslinking due to enhanced crosslinker availability, or an overall thinner shell. Conversely, capsules synthesized with 100% cyclohexane exhibited seemingly softer collapsed structures, suggesting a lower crosslinking density. In addition to these morphological alterations, the capsule size increased with increasing cyclohexane content. This phenomenon can be explained by a lower crosslinking density, resulting in a greater swelling capacity of the capsules, or generally in a less densely packed shell with higher porosity.

In addition to size and morphology, polarity changes may also affect the surface chemistry of the capsules, with changes in density and orientation of proteins in the capsule shell. Colorimetric assays were therefore used to test the capsules for the amount of accessible amine and leftover azide groups, as well as alkyne groups as an indicator of how much of the crosslinker has only reacted once, instead of crosslinking. Furthermore, investigations of the surface tension of the different solvent mixtures, as well as their interfacial tension with water, might provide insight into possible reasons for any observed trends. NMR spectroscopy was used to quantify the amount of reacted HDDP after 24 h. In order to gain insight on the degree of denaturation in the protein, nano differential scanning fluorimetry (NanoDSF) was performed. Lastly, the solvent-dependent zeta potentials were measured. The corresponding results are presented below (Fig. 5).

Amine concentrations per milligram nanocapsules were determined by fluorescamine assay (Fig. 5A, calibration curve in Fig. S10).[22] As with the size and morphology, clear trends become visible for the amine concentration with variation of the solvent concentration. With a decrease in toluene content, an increase of detectable amine groups per milligram was observed. Additionally, the number of amine groups per area was calculated, and the resulting trend matched the amine groups per milligram.

In addition to amine groups, the number of leftover, unreacted azide groups was detected using an AlexaFluor488-dibenzocyclooctyne (AF488-DBCO) dye. Defined amounts of the dye and capsules were mixed and diluted to a defined total volume, incubated overnight, and centrifuged. The fluorescence of the supernatant was measured, and used to calculate the concentration of the dye in the supernatant by comparison to a concentration series of AF488-DBCO (calibration curve in Fig. S11).

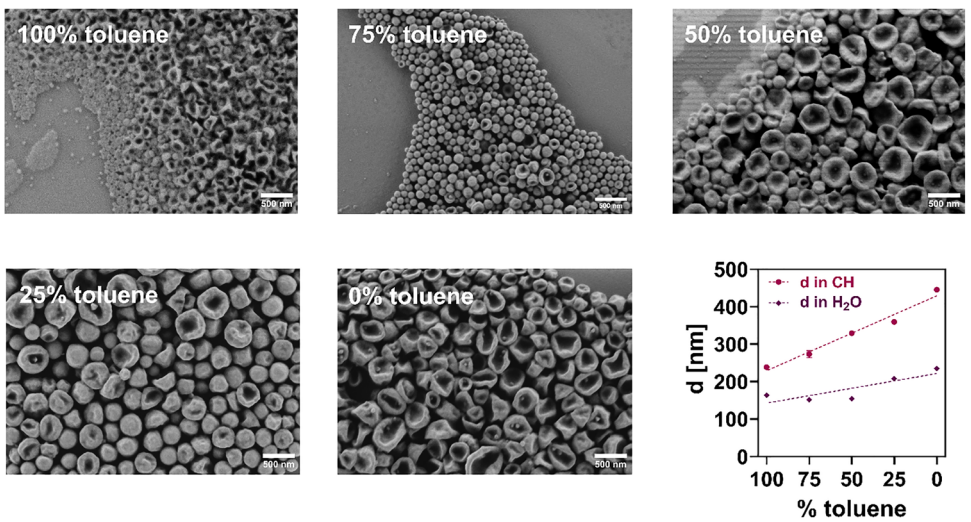

Fig. 4 Scanning electron microscopy (SEM) and dynamic light scattering (DLS) based evaluation of size, dispersity, and morphology of protein nanocapsules synthesized with 5 eq. crosslinker under variation of the solvent composition (mixtures of cyclohexane and toluene). DLS measurements were performed in triplicates (SD included as error bars). Scale bars: 500 nm.

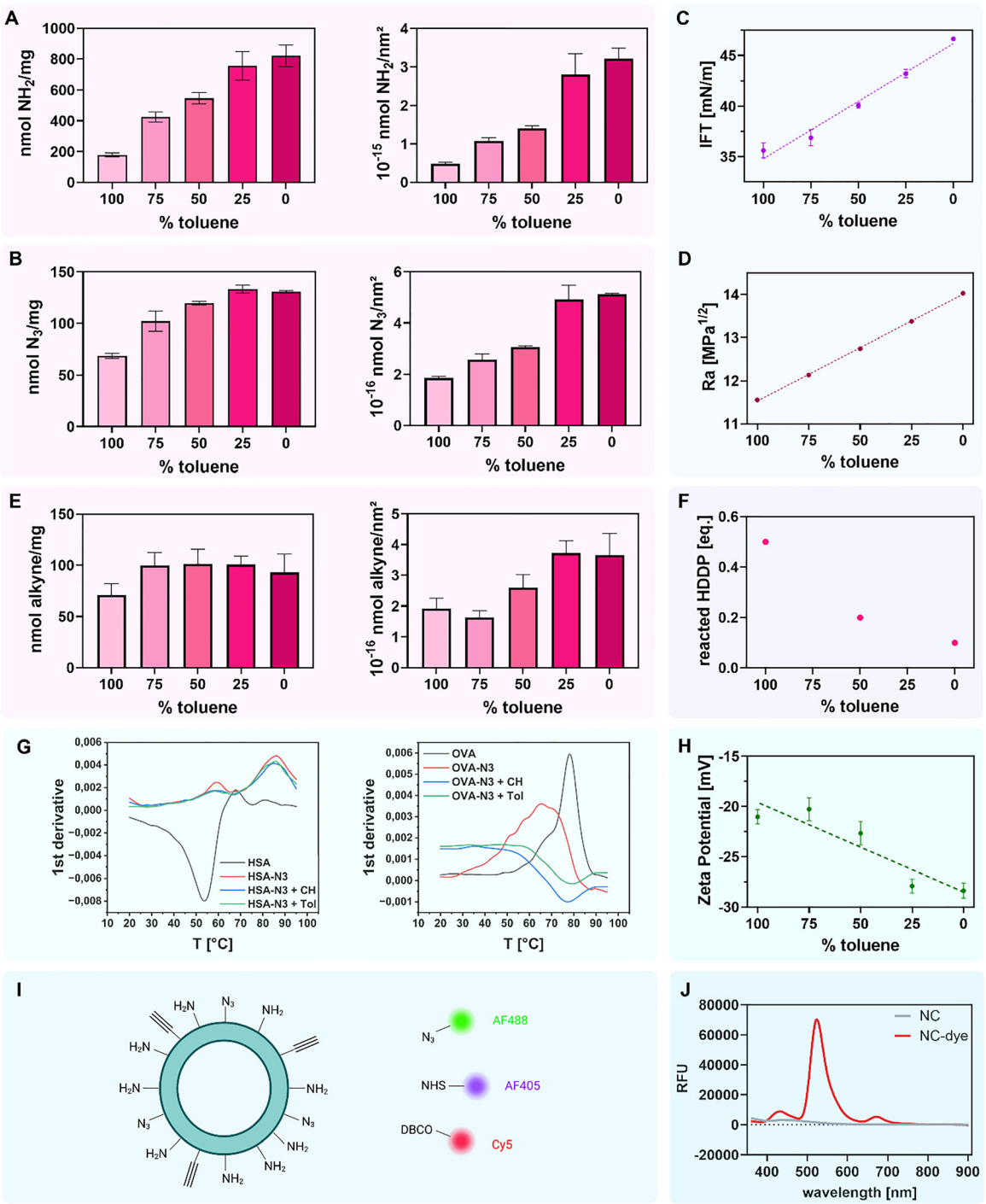

Fig. 5 Surface functional group and crosslinker reactivity characterization for protein nanocapsules synthesized with 5 eq. HDDP under variation of the solvent mixture. Solvent dependent interfacial tension, calculated HSP distance R_a, and zeta potential. NanoDSF as an indicator of denaturation. Proof of multifunctionality. (A) Amine groups per milligram NCs and per surface area groups detected *via* fluorescamine assay (measured in triplicates, SD included as error bars); (B) azide groups per milligram and per surface area measured in an inverse assay using AF488-DBCO (triplicates, SD included as error bars); (C) interfacial tension between the cyclohexane/toluene mixtures and water (measured in duplicates, SD included as error bars). (D) HSP distance of the solvent mixtures to HDDP; (E) alkynes per milligram and per surface area measured in an inverse assay using AF488-N_3 (triplicates, SD included as error bars). For calculations see SI. (F) Reacted amount of HDDP after 24 h depending on the solvent mixture (determined by observation of the decrease in the alkyne proton signal of HDDP in ^{1}H NMR spectroscopy); (G) first derivatives of NanoDSF curves measured for HSA and OVA after azidation and sonication with cyclohexane and toluene; (H) zeta potentials of the prepared NCs (measured in triplicates, displayed as mean, SD as error bars); (I) schematic representation of the proof-of-principle experiment to evaluate multifunctionality (Created in BioRender. Jung, C. (2025) **https://BioRender.com/qmu5qzf**) and (J) fluorescence spectrum confirming the successful attachment of all three dyes.

The amount of azides available for reaction was calculated as the difference between the total amount of initially added dye and the amount of dye present in the supernatant. Due to the bigger size of the dye, a deeper penetration into the capsule is unlikely, allowing for the detection of the surface groups only. As was the case with the amine groups, an increase in azide groups was detected with a decrease in toluene content (Fig. 5B). This finding further supports the hypothesis that the reaction of the crosslinker with the protein-azides is more efficient in the presence of toluene, possibly due to a higher solubility of HDDP.

The observed linear trends in surface groups match the trends in surface tension (Fig. S12) and interfacial tension (Fig. 5C), as well as the calculated distance R_a between HDDP and the solvent mixtures (according to their Hansen solubility parameters (HSPs), Fig. 5D and Fig. S13, S14, Table S2). The surface tension decreases with increasing cyclohexane content, while the interfacial tension to water increases correspondingly, although to a higher degree due to the greater difference in polarity of the organic solvents to water as opposed to air. The higher interfacial tension might impair the reactivity of the crosslinker at the interface, which would lead to a lower total reaction efficiency. This hypothesis is supported by the experimental detection of a higher amount of leftover azides with increasing cyclohexane content. This lower reaction efficiency may result in a less dense crosslinking, which could lead to a higher mobility of the shell proteins and a higher accessibility of the surface functional groups after synthesis in cyclohexane. The lower solubility and therefore availability of HDDP is further supported by the calculated increase in HSP distance with increasing cyclohexane content, for which higher values indicate lower solubilities.

In addition to crosslinking, HDDP may also react on one side only. This process is unlikely to occur in large quantities due to the close proximity of the proteins at the interface, but may still take place to a certain degree. A monofunctionalization would lead to alykne groups on the nanocapsule surface. In order to quantify this amount of alkyne groups, a colorimetric assay using AF488-N_3 was performed analogue to the azide group quantification (calibration curve in Fig. S15). The detected quantities are presented in Fig. 5E. While no clear trend emerges for the values per milligram capsule material, an increase with increasing cyclohexane content can be observed when evaluating the alkyne groups per surface area.

Furthermore, to experimentally confirm that the reactivity is responsible for the different properties of the nanocapsules, an ^{1}H NMR spectroscopy study was conducted (individual spectra in Fig. S16). Directly after addition of the crosslinker during synthesis, samples were taken and NMR spectra were measured for 24 h at 40 °C. Observation of the alkyne proton signal of the crosslinker revealed trends in HDDP reactivity, where the highest reactivity was observed in 100% toluene, with about half of the total azide amount reacting, and the lowest reactivity observed in 100% cyclohexane, with only about a tenth of the total azide amount reacting (Fig. 5F).

This trend is a possible explanation for the higher amount of mono-reacted HDDP observed in the alkyne group quantification, as the looser crosslinking may lead to a larger distance between individual proteins and, consequently, azide groups. In combination with the lower reactivity of the crosslinker itself, this increased distance explains the increased likeliness of monofunctionalization.

In order to investigate to which degree the solvent hydrophobicity impacts the degree of protein denaturation, a series of nano differential scanning fluorimetry (NanoDSF) measurements were performed, revealing that the used sonication protocol does not significantly denaturate the proteins, but that azidation causes denaturation, which progresses further when sonicating in water/organic solvent mixtures (Fig. 5G and Fig. S17, S18). However, this organic solvent driven denaturation was observed to equal degrees for cyclohexane and toluene, suggesting that denaturation processes are unlikely to result in solvent-dependent surface changes, leaving only crosslinker availability and protein orientation as deciding factors.

The zeta potential of the capsule series exhibited a decreasing trend with a reduction in toluene content (Fig. 5H). This indicates that, in addition to the amine groups (important for the linker attachment), and the azide and alkyne groups (involved in crosslinking), the total number of charged groups on the nanocarrier surface rises as the cyclohexane content increases.

The presence of multiple functional groups on the nanocarrier surface suggests that a multifunctionalization may be possible. For this purpose, the involvement of azide chemistry offers the additional opportunity of biorthogonal multifunctionalization. To prove that this is feasible, a nanocapsule synthesized without Cy5-oligo dye was functionalized with alkyne-reactive Cy5-sulfo-N_3, azide-reactive AF488-DBCO, and amine-reactive AF405-NHS (Fig. 5I, J and Fig. S19). Leftover dye was removed through extensive washing. The fluorescence spectra of the resulting nanocapsules show the presence of all three dyes, confirming that the nanocapsules are accessible to functionalization by multiple groups in orthogonal reactions.

3.2 Biological interaction

In addition to studying how the solvent affects the physical and chemical properties of the capsules, it is important to understand their biological fate, especially since they are designed for biological and medical uses like delivering drugs, antigens, or adjuvants.[9] A thorough evaluation of the protein corona and cell uptake into macrophages was therefore performed (Fig. 6).

3.2.1 Protein corona analysis. Since the protein corona is known to significantly affect the cellular interaction of nanocarriers, altering their biological identity and either promoting or impeding uptake into cells, an investigation of its composition was performed. To capture the expected differences in protein adsorption arising from their contrasting surface functionalities, the samples prepared with 100% and 0% toluene were specifically chosen for analysis. The significantly higher amine group density—approximately eightfold in the sample prepared in cyclohexane (see Fig. 5B)—is likely to cause considerable differences in both the quantity of adsorbed proteins and the types of proteins that bind. Both samples were

incubated in human citrate plasma and subsequently washed to remove the loosely bound soft protein corona. The hard protein corona remaining on the nanocapsule was then desorbed by treating with an SDS-based solution, digested, and evaluated using liquid chromatography mass spectrometry (LC-MS). The relative frequencies of the protein groups, exact percentages of selected components, and the twenty most abundant proteins are presented in a heat map in Fig. 6A–C.

Similar total protein amounts of about 20 μg mg^{-1} NCs without, and 30 μg mg^{-1} NCs with human plasma incubation

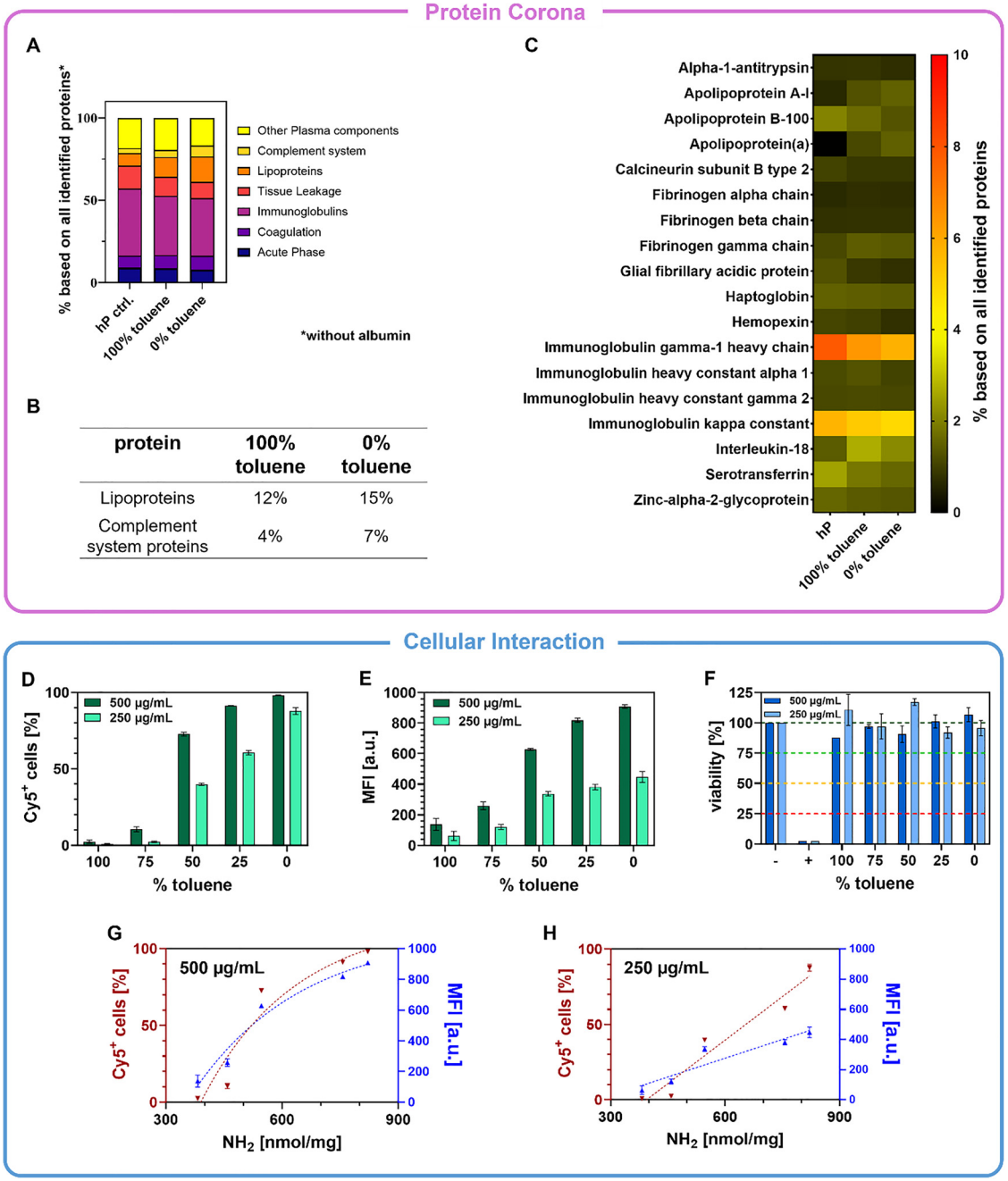

Fig. 6 Evaluation of protein absorption and cellular interaction. (A)–(C) For the protein corona, only samples prepared with 100% and 0% toluene were compared, as they were expected to show the most pronounced differences. (A) Summary of identified protein groups and their relative abundancies, excluding HSA and OVA. (B) Relative abundancies for selected protein groups. (C) Heat map of the 20 most abundant proteins detected in the protein corona, excluding HSA and OVA. (D)–(H) Cellular uptake of the prepared protein NCs. Uptake was performed in triplicates in J-774A.1 cells at 250 μg mL^{-1} and 500 μg mL^{-1} over 18 h at 37 °C. Samples were evaluated *via* flow cytometry for uptake, and CellTiter Glo™ Assay for viability. SD as error bars. (D) Percentage of $Cy5^+$ cells in dependency of the toluene amount in the initial synthesis. (E) Corresponding mean fluorescent intensities (MFIs). (F) Cell viabilities relative to untreated (–) and 20% DMSO treated (+) cells. (G)–(H) $Cy5^+$ cells and MFIs in dependency on amine group amount detected on the capsule surface.

were observed for the two samples (Fig. S20). When comparing the relative frequencies of the proteins grouped according to function, the differences between the two nanocapsule samples are only minor (Fig. 6A). Relevant proteins and protein groups are presented in Fig. 6B. Since the nanocapsules were prepared from HSA and OVA, the two proteins were excluded from the evaluation.

Comparing the 100% toluene sample to the 0% toluene sample reveals a slight increase in lipoprotein content from 12% to 15%. Although lipoproteins are considered dysopsonins (stealth proteins) due to their ability to reduce cellular uptake, this effect typically occurs only at higher concentrations, which are not reached in either sample. In contrast, complement proteins act as opsonins and promote cellular uptake; however, the 3% increase observed in the 0% toluene sample is likely too small to significantly affect cellular interactions.

The observed differences in protein corona are negligible for the two samples, and the protein corona alone is unlikely to cause significant variations in cell uptake. However, it is important to note that it is one of several factors influencing the cellular interactions of the nanocapsules, and other variables, such as surface charge, might still affect cellular interaction and result in observable differences in cell uptake, necessitating *in vitro* investigations.

3.2.2 *In vitro* assays. *In vitro* assays were performed in macrophages to examine the impact of altering the solvent and the corresponding change in surface properties on cellular interaction. Here, the cellular uptake and viability were evaluated after an incubation period of 18 h for two concentrations of the capsules in the medium, namely 500 μg mL^{-1} and 250 μg mL^{-1}. The corresponding results are presented in Fig. 6D–H.

As opposed to the protein corona absorption, the variation in surface properties leads to major alterations in the nanocapsule cell interaction. As the toluene content is reduced, there is a pronounced increase in the percentage of cells that have taken up nanocapsules (Fig. 6D). This trend is evident for both concentrations, although the increase is linear with the cyclohexane percentage for the 250 μg mL^{-1} condition, while saturation is reached for the 500 μg mL^{-1} condition, resulting in a plateau. A comparable trend is observed in the median fluorescence intensities (MFIs, Fig. 6E), which increase noticeably as the toluene content decreases. Importantly, none of the samples showed any signs of toxicity at either concentration tested (Fig. 6F). All viabilities reached values above 80%, even at relatively high concentrations. Together with the biodegradability of the capsule material,[7] these findings are promising for the intended use of the presented nanocapsule system for nanomedical applications. The nature of the crosslinking reaction which forms the nanocapsule shell ensures little to no cross-reaction with a wide variety of cargos, making this nanocarrier type an ideal drug delivery vehicle, with the adjustable amine group density acting as a passive targeting, or allowing for the controlled attachment of further active targeting moieties.

In addition to the dependence of the cell uptake on the solvent mixture, it can also be evaluated relative to the amine group density (Fig. 6G and H). A linear increase in the percentage of nanocarrier-positive cells and the MFI with the amine concentration was observed for the lower nanocarrier concentration, while a plateau was observed for the higher concentration. These trends align closely with those depicted in Fig. 6D and E.

This substantial variation in cell uptake intensity, depending on the hydrophobicity of the continuous phase in nanocapsule synthesis, underscores the profound impact of solvent choice on cell uptake and the potential for inducing a stealth effect or enhancing uptake by the surface charge. Notably, capsules synthesized in toluene exhibit minimal uptake even at high concentrations, yet retain a substantial amount of accessible surface functional groups, rendering them highly promising candidates for functionalization with targeting moieties.

4 Conclusion

In this study, we systematically varied reaction parameters in the inverse miniemulsion-based synthesis of protein nanocapsules, and investigated their influence on the capsule properties. A key finding is the strong effect of the continuous phase hydrophobicity, modulated by varying the ratio of toluene and cyclohexane, on the capsule size and surface chemistry. With increasing cyclohexane content, a marked rise of amine density per surface area was observed, along with the presence of additional functional groups. The observed trends can be attributed to changes in solubility and reactivity of the crosslinker, as well as the altered protein orientation at the water-to-oil interface affecting the accessibility of functional surface groups. The presence of multiple surface groups enables multifunctionalities of the nanocapsule, as demonstrated in a proof-of-concept experiment. While surface chemistry changes had only a modest impact on protein corona formation, macrophage uptake studies revealed a pronounced influence of solvent composition on nanocarrier–cell interactions. A positive correlation between surface amine content and cellular uptake intensity suggests that solvent variation offers a strategy to modulate biological behavior, including potential stealth effects. Moreover, the ability to fine-tune the functional group density opens up new possibilities for precise conjugation of targeting ligands like antibodies and nanobodies. Optimizing their density could enhance targeting efficieny and reduce the required therapeutic dose in nanocarrier-based drug delivery.

Author contributions

The manuscript was written through contributions of all authors. All authors have given approval to the final version of the manuscript.

Conflicts of interest

There are no conflicts to declare.

Data availability

The data supporting this article have been included as part of the supplementary information (SI). Supplementary information: IR and NMR data, solubility trials, DLS, zeta potential, calibration curves, NanoDSF, surface tension, HSP, additional protein corona data, fluorescence spectra, absorbance spectra. See DOI: **https://doi.org/10.1039/d5nh00563a**.

Acknowledgements

We gratefully acknowledge the Deutsche Forschungsgemeinschaft (SFB1066), the Leibniz-Wissenschaftscampus NanoBrain (Project number: W71/2022) and the Carl Zeiss Foundation (Nano@Liver) for funding. XY was funded by the Chinese Scholarship Council (CSC). We would like to thank Gunnar Glaßer for SEM measurements, Christoph Siebert and Kathrin Kirchhoff for TEM measurements, Ute Heinz for NanoDSF measurements and surface and interfacial tension measurements, Sandra Seywald for surface and interfacial tension measurements, and Dr rer. nat. Manfred Wagner and Stefan Spang for their assistance with the NMR spectroscopy measurements and evaluation. This text was checked with DeepL Write and changes were evaluated for each suggestion of DeepL Write.

References

1 (*a*) Y. Li, M. Kröger and W. K. Liu, *Nanoscale*, 2015, **7**, 16631; (*b*) X. Jiang, A. Musyanovych, C. Röcker, K. Landfester, V. Mailänder and G. U. Nienhaus, *Nanoscale*, 2011, **3**, 2028; (*c*) A. Villanueva, M. Canete, A. G. Roca, M. Calero, S. Veintemillas-Verdaguer, C. J. Serna, M. del Puerto Morales and R. Miranda, *Nanotechnology*, 2009, **20**, 115103; (*d*) H. Jin, D. A. Heller, R. Sharma and M. S. Strano, *ACS Nano*, 2009, **3**, 149.

2 V. Holzapfel, A. Musyanovych, K. Landfester, M. R. Lorenz and V. Mailänder, *Macromol. Chem. Phys.*, 2005, **206**, 2440.

3 (*a*) A. K. Gupta and M. Gupta, *Biomaterials*, 2005, **26**, 3995; (*b*) R. P. Bagwe, L. R. Hilliard and W. Tan, *Langmuir*, 2006, **22**, 4357.

4 (*a*) J. Simon, M. Fichter, G. Kuhn, M. Brückner, C. Kappel, J. Schunke, T. Klaus, S. Grabbe, K. Landfester and V. Mailänder, *Nano Today*, 2022, **43**, 101375; (*b*) C. Jung, M. Fichter, J. Oberländer, J. Schunke, V. Bolduan, P. Schneider, J. Kang, K. Koynov, V. Mailänder and K. Landfester, *Adv. Mater.*, 2024, 2412563.

5 A. M. Alkilany, L. Zhu, H. Weller, A. Mews, W. J. Parak, M. Barz and N. Feliu, *Adv. Drug Delivery Rev.*, 2019, **143**, 22.

6 A. Brouillard, N. Deshpande and A. A. Kulkarni, *Adv. Healthcare Mater.*, 2021, **10**, 2001680.

7 N. Hüppe, J. Schunke, M. Fichter, V. Mailänder, F. R. Wurm and K. Landfester, *Nanoscale Horiz.*, 2022, **7**, 908.

8 Z. Ya, Y. Hailemichael, W. Overwijk and N. P. Restifo, *Curr. Protoc. Immunol.*, 2015, **108**, 20.1.1.

9 J. Schunke, N. Hüppe, N. Mangazeev, K. R. Speth, K. Rohde, F. Schön, V. Bolduan, P. Schneider, T. Klaus, M. Kuske, S. Grabbe, K. Landfester, V. Mailänder and M. Fichter, *Nano Today*, 2024, **57**, 102365.

10 T. Prenzel, M. Wilhelm and K. Rezwan, *Chem. Eng. J.*, 2014, **235**, 198.

11 (*a*) H. Wang, Q. Zou, O. C. Boerman, A. W. G. Nijhuis, J. A. Jansen, Y. Li and S. C. G. Leeuwenburgh, *J. Controlled Release*, 2013, **166**, 172; (*b*) D. T. Pham, N. Saelim and W. Tiyaboonchai, *Colloids Surf., B*, 2019, **181**, 705; (*c*) D. T. Pham, N. Saelim and W. Tiyaboonchai, *J. Mater. Sci.*, 2018, **53**, 14087.

12 R. A. Bradshaw, A. L. Burlingame, S. Carr and R. Aebersold, *Mol. Cell. Proteomics*, 2006, **5**, 787.

13 M. Kokkinopoulou, J. Simon, K. Landfester, V. Mailänder and I. Lieberwirth, *Nanoscale*, 2017, **9**, 8858.

14 J. C. Silva, M. V. Gorenstein, G. Z. Li, J. P. Vissers and S. J. Geromanos, *Mol. Cell. Proteomics*, 2006, **5**, 144.

15 E. Stefanis and C. Panayiotou, *Int. J. Thermophys.*, 2008, **29**, 568.

16 M. Mihalovits, *J. Mol. Liq.*, 2022, **364**, 119911.

17 (*a*) S. Tenzer, D. Docter, S. Rosfa, A. Wlodarski, J. Kuharev, A. Rekik, S. K. Knauer, C. Bantz, T. Nawroth, C. Bier, J. Sirirattanapan, W. Mann, L. Treuel, R. Zellner, M. Maskos, H. Schild and R. H. Stauber, *ACS Nano*, 2011, **5**, 7155; (*b*) D. Hofmann, S. Tenzer, M. B. Bannwarth, C. Messerschmidt, S. F. Glaser, H. Schild, K. Landfester and V. Mailänder, *ACS Nano*, 2014, **8**, 10077.

18 E. Fröhlich, *Int. J. Nanomed.*, 2012, **7**, 5577.

19 M. J. Roberts, M. D. Bentley and J. M. Harris, *Adv. Drug Delivery Rev.*, 2002, **54**, 459.

20 N. Hueppe, F. R. Wurm and K. Landfester, *Macromol. Rapid Commun.*, 2023, **44**, 2200611.

21 (*a*) P. P. Batra, M. A. Roebuck and D. Uetrecht, *J. Protein Chem.*, 1990, **9**, 37; (*b*) C. Muste and C. Gu, *Drug Metab. Pharmacokinet.*, 2022, **42**, 100433.

22 M. Gai, J. Simon, I. Lieberwirth, V. Mailänder, S. Morsbach and K. Landfester, *Polym. Chem.*, 2020, **11**, 527.